IEEE Open Journal of
Antennas and Propagation

Received 7 August 2020; revised 14 September 2020; accepted 14 October 2020. Date of publication 2 November 2020; date of current version 4 December 2020.

Digital Object Identifier 10.1109/OJAP.2020.3035196

Practical Diversity Design for PCB IoT Terminals

MARYAM RAZMHOSSEINI (Student Member, IEEE), ABHIJIT BHATTACHARYA, (Member, IEEE), AND RODNEY G. VAUGHAN (Life Fellow, IEEE)

Department of ENSC, Simon Fraser University, Faculty of Applied Sciences, ENSC, Burnaby, BC V5A 1S6, Canada
M. Razmhosseini and A. Bhattacharya contributed equally to this work.
CORRESPONDING AUTHOR: M. RAZMHOSSEINI (e-mail: mrazmhos@sfu.ca)

This work was supported by the Natural Sciences and Engineering Research Council of Canada (NSERC) under Grant RGPIN-2016-06373.

ABSTRACT Mobile or nomadic diversity antennas feature a variety of element types and layouts, mostly PCB-based, reflecting complex design trade-offs between their performance and the required compactness. The design stage is electromagnetic-based but must include several signal-based diversity metrics, and there is a shortfall of information about their assumptions and the impact of their violation. The evaluation stage normally includes simulation, with physical measurements being the bottom line. Pattern measurement is particularly challenging, but accurately measured patterns are critical parameters, enabling the calculation of mean gains and correlations, and the impact of different propagation scenarios. For developers, the complex set of processes for design and evaluation make it difficult to have confidence with their in-house procedures without access to independent results for a variety of antenna types. For the design stage, we review and clarify the diversity metrics, and for evaluation, a set of typical and new diversity designs implemented on printed circuit board (PCB) are also presented. The methods cover lossy antennas and the expected performance in a directional propagation scenario. This information helps designers and developers to better understand the design process and to check their evaluation procedures.

INDEX TERMS Mobile antennas, diversity performance benchmarks, MIMO, Internet-of-Things, 5G, von-Mises Fisher distribution, directional propagation.

I. INTRODUCTION AND BACKGROUND

DIVERSITY/MIMO systems are key technologies for mobile communications where increasing capacity calls for an increase in the number of antennas on compact mobile terminals. In current and future systems, the Internet-of-Things (IoT) includes a wide variety of mobile or nomadic wireless devices. The antennas in these systems are mainly PCB-based because of their low cost, and so PCB (or LCP [1]) implementations are used in this article. We review and clarify the often-confusing diversity metrics and demonstrate them for a set of PCB antennas typical of those used in IoT terminals. This information allows designers and researchers to check their procedures, code, and testing equipment, for performance evaluation. The designs include lossy antennas, feed effects, and directional propagation scenarios.

Essentially all mobile and nomadic systems have multipath channels which is where diversity [2]–[10] can be so powerful. When there is little multipath degradation, diversity is not required, and the classical maximized directional gain - spatial point-to-point - is appropriate. The mechanism of diversity is essentially the same as the classical point-to-point gain maximization, but instead of maximizing the gain to single direction, the gain is maximized to a wanted signal (or a signal-to-interference ratio) which has distributed, or multipath, directions. The principle of diversity is transmission through channels with different multipath degradations and using a combination of these channels to improve the communications performance.

From the communications viewpoint, diversity strives for a maximum number of channels with uncorrelated degradation and with similar mean gains so that each of the channels is equally contributing on average. From the antenna designer's viewpoint, we strive to populate the terminal with a maximum number of elements to maximize the number of diversity channels. But an increasing number of antennas on a fixed-size terminal trades off with increasing correlation, increasing mutual coupling, and a decreasing bandwidth and efficiency, - all of which degrade the performance. The goals of the communications designer and the antenna designer have dissimilar languages, but

there is overlap in the evolving set of diversity metrics. These metrics are not all clear-cut to apply or interpret because the assumptions for, and relationships between, the metrics are not widely reported. Consequently, developers are often unsure of their evaluations because of the complexity of the combination of electromagnetic, signal processing, and communications factors. This motivates: (i) a review of these metrics; and (ii) reporting the results of a set of basic designs so that developers can check their in-house performance estimates against such known results.

Finally, communications performance is often evaluated by "Over The Air" (OTA) tests. These give a throughput for a whole system, including the antennas, their adaptive combining algorithms, and the communications signal processing, all operating within a physically synthesized model propagation scenario. An OTA measurement cannot separate these individual aspects, so the performance of a new antenna design cannot be readily separated from other performance-limiting components. Also, the accuracy of the physically synthesized multipath channel model (e.g., using a reverberation chamber) is difficult to verify, so this becomes part of the antenna measurement uncertainty. For the mobile or nomadic device antenna designer, understanding and interpreting the diversity metrics is critical, and is a motivation for this work.

A recent work [11] on measured pattern evaluation uses the pattern spatial correlation function of an optically fed (to avoid cable scattering in pattern measurement), wideband, biconical antenna. While the approach offers extraordinary evaluation accuracy, such an antenna is not normally used for devices.

This article addresses antenna performance evaluation of device antennas, i.e., PCB antennas. The new contributions include: the discussion and interpretation of the various diversity metrics; benchmark antenna designs and their new results with numerical and physical measurements to gauge their similarity and check evaluation processes; lossy antenna considerations; a new diversity antenna design using a daughter board attached to the PCB; and the use of a 3D directional scenario (we introduce the von-Mises Fisher distribution for this) to model the impact of unimodal directionality on the performance metrics. These benchmark antennas are simple to model and construct and with their details provided, they are readily reproduced.

Section II reviews the mobile antenna performance metrics, including communications capacity for multipath channels. Section III presents 5 benchmark PCB-based designs, where a lot of information is supplied on antenna performance graphs so that designers can use these to check their results from their own evaluation systems. Section IV looks at the related propagation and capacity aspects, including the use of a new PCB-based design. Section V shows how to characterize the impact of 3D propagation directionality.

II. DIVERSITY/MIMO SYSTEM EVALUATION METRICS

A. ENVELOPE CORRELATION COEFFICIENT (ECC)

The correlation matrix of a diversity antenna governs its communications performance and has become the most important metric for a diversity/MIMO antenna. It contains the envelope correlations between the elements, with the mean element gains (autocorrelations) on the diagonal. In communications, the correlation represents the similarity between the fading envelopes of narrowband diversity channels, which explains its name. The pioneering treatments on diversity, e.g., [2], [3], reviewed in [12], considered a time- (or space-) function of the Rayleigh-like envelopes of the changing channels. In practice, sampling and recording this spatial function as a time-series where the terminal has a varying speed or orientation, is complicated. For any large-scale physical mobile experiment, being able to reproduce such an experimental series calls for an extremely complicated set-up. Physical experiments are therefore from statistical estimates, and the reproducability is confined to statistical-based comparisons. The way forward has been to express an ECC via an inner product of the various antenna elements' complex patterns, where the inner product weighting (cf., its pdf) is a statistical propagation scenario model. This inner product is well-defined, repeatable (in the sense that the pattern measurements can be repeated), and allows different, and even varying, propagation scenarios to be included, so it has become the key tool for diversity antenna design. The name ECC remains associated with the pattern inner product formulation, although it is different to its time- of spatial-series prototype because of the modeling assumptions/simplifications required for the inner product formulation. For a particularly simplified propagation model (far-field situation, minimum-scattering-like elements, uniform, angularly uncorrelated multipath in each polarization, uncorrelated multipath between polarizations, and with the polarizations of equal power), the pattern inner product form of the ECC can be expressed in terms of the mutual resistance between lossless antennas [4], [13]. The advantage of such an impedance formulation is that, as antenna parameters, the port impedances can be readily measured, and the experiments reproduced very simply. In a simulation or measurement, the impedance matrix is calculated from the primary measurement parameters, i.e., the scattering parameters, and instead of expressing the mutual impedance by name, using the equivalent (e.g., [14]) scattering parameter expression [15], [16] has been popular. Antenna patterns are perhaps the most difficult parameter to measure, requiring expensive equipment which can be afforded only by larger companies and institutions. Patterns from simulation are much more convenient but there is no guarantee that these accurately represent the true patterns. Similarly, impedances can be readily found from simulation, but their physical measurement requires a vector network analyzer and a test set-up with suitable antenna clearance from scatterers. The great advantage of simulation is that it can provide visualization

of the fields and currents, and allows quick parametric studies for design. The shortcomings of relying on simulated results are that we cannot be sure that the simulation model for the antenna itself is correct, and that the patterns and impedances of antennas on compact terminals depend on the terminal detail and the immediate surroundings which are seldom part of the simulation model.

The envelope (as in the term ECC) is used because traditional analogue receivers often have a real-time, analogue RSSI signal available, and the correlations of this power signal (viz., envelope squared, with its correlation denoted ρ_{e^2}) is closely related to the envelope correlation coefficient, denoted ρ_e. The power signal is easier to get from hardware and is an easier form to deal with in statistical signal processing. With digital receiver architectures, the complex channel signal can be available, and the correlation coefficient between these complex channel signals, ρ, is also related to the envelope correlation coefficient, by $|\rho\ |^2 \approx \rho_e \approx \rho_{e^2}$. So the ECC is taken as the magnitude square of its complex Gaussian version, ρ, e.g., ECC between the i^{th} and j^{th} branches is $\rho_{eij} = |\rho_{ij}|^2$.

A zero correlation is best of course. A negative correlation would be even better for the diversity gain (see below), but for Rayleigh envelopes, the envelope correlation coefficient is not negative, although its estimate can be negative owing to the finite duration of the signals used for the estimation. For small-dimensioned diversity antennas (just a couple of elements), a "high" correlation (coefficient well over 0.5) still gives strong performance improvement for most diversity applications [2]–[4], [17]. But for larger numbers of elements, even moderate correlations degrade communications performance metrics such as capacity, e.g., [18]. The one-sided frequency support for the frequency correlation coefficient function to be over some threshold, such as $\rho_e = 0.5$, is called the correlation bandwidth, and this is used below for frequency diversity design. This is analogous to using the correlation distance between spaced antennas for space diversity design.

In the derivation of the pattern inner product expression for ECC, key assumptions include the following. (i) The distributed propagation model is identical for each antenna element. This means that the patterns considered are far-field only, and that there are no close-proximity scatterers. In a cellphone, the hands, head, and even torso, can act as close-proximity absorbing scatterers, and the pattern should strictly include the effects of these scatterers as part of the complex mobile platform. For indoor situations, proximate wall-, floor- and ceiling-borne scatterers can be part of the complex platform. (ii) The propagation is: statistically stationary; (iii) perfectly uncorrelated between polarizations; and (iv) between all angles in each polarization. For the special case of using the impedance-based formulation (i.e., the s-parameters) for the ECC, both the polarizations must also be of equal power and uniformly distributed, and the antennas must be lossless.

1) ECC FROM THE ANTENNA PATTERN INNER PRODUCT

The pattern inner product between the ith and jth ports is found from ECC = $\rho_e = |\rho_{ip}|^2$, where

$$\rho_{ip}^{(non-u)}\left(P, h_i h_j\right) = \frac{\oiint_{4\pi} H_{i,j}(\Omega) d\Omega}{\sqrt{\oiint_{4\pi} H_{i,i}(\Omega) H_{j,j}(\Omega) d\Omega}}, \qquad (1)$$

in which Ω is the solid angle with $d\Omega = sin\theta d\theta d\phi$, $H_{i,j}(\theta, \phi) = XPR.h_{\theta,i} h^*_{\theta,j} P_\theta + h_{\phi,i} h^*_{\phi,j} P_\phi$, with $h_\theta(\theta, \phi)$ and $h_\phi(\theta, \phi)$ the normalized patterns in the θ and ϕ polarizations, respectively, $P_\theta(\theta, \phi)$ and $P_\phi(\theta, \phi)$ are the θ and ϕ polarization pdfs of the multipath, and XPR is a cross-polarization ratio (the ratio of the total $\theta-$ and $\phi-$ polarized powers of the propagation scenario).

The pattern inner product formulation allows the impact of various propagation scenarios (i.e., polarized, non-uniform, or *non-u*), to be studied, and allows lossy antennas in the sense that the patterns can be of the embedded elements so that the mutual coupling effects, ohmic loss, and mismatch loss are included. For these reasons, this formulation is more general than the s-parameter formula, and more accurate in practice.

For uniformly distributed power in each polarization, and equal powers in each polarization, ($XPR = 1$) the simplication is $P_\theta = P_\phi = 1$, the correlation can be denoted $\rho_{ip} = \rho^{(u)}$, and this most popular statistical model is also used below.

In our pattern correlation calculations below (Section III), the angular sampling density is maintained to ensure that the calculation accuracy is negligible compared to the experimental error. This needs to be checked on a case-by-case basis since the sampling density is governed by the complexity (cf., spherical mode content) of the patterns.

2) ECC CALCULATION FROM IMPEDANCE

The correlation coefficient between open-circuited voltages of MSA-like antennas can be expressed as the normalized mutual resistance, $\rho_{o,ij} = E(V_{oi} V_{oj}^H) = r_{ij} = R_{ij}(R_{ii} R_{jj})^{-1/2}$ and this can in turn be related to the loaded-circuit case by $\rho_{L,ij} = \rho_{ij} = F \rho_{o,ij} F^H$ in which $F = Z_L(Z_A + Z_L)^{-1}$. The simplifications required for the impedance expression can lead to incorrect results where the assumptions are violated, for example when the antennas are lossy or the propagation scenario is not uniform.

3) ECC CALCULATION USING SCATTERING PARAMETERS

The use of the s-parameter expressions [15], [16] for the impedance expression has made this form popular. Recalling that ECC = $\rho_{eij} = |\rho_{ij}|^2$, the formula for the n-port case is [19], [20]

$$\rho_{ij} = -\frac{\sum_{n=1}^{N} S^*_{ni} S_{nj}}{\sqrt{\left(1 - \sum_{n=1}^{N} |S_{ni}|^2\right)\left(1 - \sum_{n=1}^{N} |S_{nj}|^2\right)}}. \qquad (2)$$

B. PATTERN FREQUENCY CORRELATION FUNCTION (PFCF)

Instead of using spaced antennas, which often means a less compact terminal to cater for the diverse antennas, the same antenna can be used at diverse frequencies. This is sometimes called frequency diversity, or multipath diversity [2], [12], [21]. Note that using extra bandwidth in this way does not help with the capacity efficiency ("C/B" in traditional communications engineering, but also referred to as just capacity, "C", from information theory). The PFCF is the normalized inner product between the patterns at different frequencies, and its correlation bandwidth gives the frequency spacing required for frequency diversity for a given antenna. A simple model for the total frequency correlation coefficient function, is

$$\rho_{Total}(\Delta f) = \rho_{h_{Tx}}(\Delta f) \cdot \rho_{\tilde{H}}(\Delta f) \cdot \rho_{h_{Rx}}(\Delta f) \tag{3}$$

where $\rho_{h_{TX}}$, $\rho_{h_{RX}}$ and $\rho_{\tilde{H}}$ are the frequency correlation coefficients of: the transmit (Tx) antenna pattern; the receive (Rx) antenna pattern; and the propagation channel transfer functions, denoted $\rho_{\tilde{H}}(\Delta f; f_0) = \tilde{H}(f_0)\tilde{H}^*(f + \Delta f)$. The antenna terms of Eq. (3) are the PFCF [12],

$$\rho_h(\Delta f) = \frac{|\int P(\Omega) h(\Omega, f_0) \bullet h^*(\Omega, f_0 + \Delta f) d\Omega|}{\sqrt{\int P(\Omega)|h(\Omega, f_0)|^2 d\Omega \int P(\Omega) h|\Omega, f_0 + \Delta f|^2 d\Omega}} \tag{4}$$

where here $P_\theta(\Omega) = P_\phi(\Omega) = P(\Omega)$ and $\bullet$ denotes the inner product of the patterns $h = h_\theta\hat{\theta} + h_\phi\hat{\phi}$. Recall that the envelope correlation version of this is related by $\rho_e = |\rho_h|^2$.

C. MEAN EFFECTIVE GAIN (MEG)

By inserting the same antenna voltages in the pattern inner product equation, the resulting autocorrelation gives the expected power of that single antenna, viz., the MEG [22]. It corresponds to the distributed gain of an antenna,

$$MEG = \oiint_{4\pi} \left\{ \frac{XPR}{1 + XPR} G_\theta P_\theta + \frac{1}{1 + XPR} G_\phi P_\phi \right\} d\Omega \tag{5}$$

where G_θ and G_ϕ are the polarized power gain patterns. In the special case of the uniform scenario, the MEG is half of the radiation efficiency, independent of the pattern shape. The factor of half is because the uniform propagation scenario power is divided equally between the two polarizations, and a single port antenna is polarized, i.e., can receive one polarization. If all of the power of the propagation scenario is co-polarized with the antenna, then the MEG would be the radiation efficiency. The MEG is a special case (viz., uniform, or "full sphere") of the distributed directivity or gain [4].

D. DIVERSITY GAIN (DG)

The MEGs and correlations govern diversity performance, and a combined metric is the diversity gain (DG) [2]. It can be defined as the improvement in the averaged SNR from the combined signals of a set of diversity elements, relative to the SNR from the best of the elements (or some other reference antenna such as a dipole) [4]. The DG is conditioned by a probability that the SNR of the combined branches is above a reference level. There is no standard for the probability, and it can be taken as 0.5%, for example [17]. The antenna diversity can be deployed, in principle, at either the transmit or receive end of a link, but in practice, the receive end is simpler because the channel can be estimated from the received signals.

Note that our DG definition is different [18] to a form of DG often used in communications, where it stems from the slope of a capacity or BER curve for a diversity system for a given SNR. Since this slope is also governed by the propagation (e.g., Rician, Suzuki, etc.), it can be independent of the diversity situation, so this definition does not necessarily relate to antenna performance. Our DG is defined by

$$DG_{DIV(dB)} = \left[\frac{\gamma_C}{\Gamma_C}(dB) - \frac{\gamma_{ref}}{\Gamma_{ref}}(dB) \right]_{\text{given probability}} \tag{6}$$

where γ_C is the instantaneous SNR of the combined received signal and Γ_C is its mean, $\Gamma_C = \langle \gamma_C \rangle$. Similarly, γ_{ref} and Γ_{ref} are respectively the instantaneous and mean SNR received by a single element reference antenna; $\Gamma_{ref} = \langle \gamma_{ref} \rangle$. Different types of antenna signal combining such as selection- and switched-combining (these are called non-simultaneous combining), and simultaneous combining such as maximum ratio combining (MRC), equal gain combining, all yield different DGs. So, the antenna combining is not an antenna parameter *per se*, but is a critical parameter of the antenna system.

For many real-world antenna terminals, the diversity branch powers (MEGs) are unequal and correlated (ECC non-zero). For such cases, the DG can still be calculated for MRC, and then other combining techniques can be calculated from this [2], [3], [13], [17], [23]. The DG for M MRC Rayleigh uncorrelated channels is from the cumulative density function,

$$P_{MRC}(\gamma_r \le x) = \sum_{n=1}^{M} \frac{1}{\epsilon_n} \Gamma_n \left(1 - e^{-x/\Gamma_n}\right) \tag{7}$$

where $\epsilon_n = \Gamma_n \prod_{\substack{m=1 \\ m \neq n}}^{M} (1 - \frac{\Gamma_m}{\Gamma_n})$. This allows calculation of diversity gain by using the eigenvalues of a correlation matrix containing non-zero cross-correlations. Specifically, a correlation coefficient matrix (ρ) can be orthogonalized using SVD, here interpreted as returning the non-zero singular values $[\Gamma_1 \Gamma_2 \cdots \Gamma_m]^T = SVD(\rho)$ in which $m \le M$ is the number of non-zero effective branch gains. This formula is simplified (only for simple poles in the residues in the Laplace transform of the defining characteristic function [2]) for the case $\Gamma_n \neq \Gamma_m$ meaning that the branches must have unequal mean SNRs, or MEGs. A useful metric for communications-oriented interests, is an *effective order of diversity* which is the equivalent number of ideal (uncorrelated, equal gain) diversity branches for a given antenna design in a uniform scenario [23]. Finally, a variation of

the DG is the Diversity Antenna Gain (DAG) [24], which is a combination of the MEG and a different definition of diversity gain, and ends up being the same as the DG above.

E. CHANNEL CAPACITY

This section is to help get the antenna designer on the same page as the communications signal processing designer. There are many different types of capacity, stemming from information and communications theory. MIMO performance is usually characterized by a parallel channels capacity (see, [25]–[27]) metric, in bits per channel use, which is often interpreted as bits/sec/Hz. It is helpful if the antenna developer can understand the basics of capacity and how it relates to design. MIMO systems deploy antenna diversity, in general at both ends of the link. If the channels are known (see below) at the transmitter, then the spatial resource of the antennas enables parallel, independent channels (eigenchannels), to simultaneously share the spectral resource. The sets of weights for each eigenchannel suppress coupling to the other eigenchannels so the accuracy of the weights must be consummate with the required coupling suppression.

The capacity formulation below is for a system with N_r receive antennas and N_t transmit antennas, with $N_r \geq N_t$, so that the channel martrix, $\mathbf{H}$, is $(N_r \times N_t)$.

From the usual linear channel notation, $\mathbf{y} = \mathbf{Hx} + \mathbf{n}$, $\mathbf{H}$ contains the complex gains between all of the combinations of the transmitted and received signals, and we can simplify this as depending only the antennas and the propagation. The Gram matrix, $\mathbf{HH}^+$, is $(N_r \times N_r)$, and $\mathbf{H}^+\mathbf{H}$ is $(N_t \times N_t)$, (the superscript, $+$, denotes conjugate transpose) and so it is straightforward to adapt to the case of more transmit antennas than receive antennas, sometimes called "massive MIMO" when N_t is large. The $k \leq N_t \leq N_r$ real, positive eigenvalues of $\mathbf{HH}^+$, here denoted by $\tilde{\lambda}_i$, correspond to eigenchannel power gains. The remaining eigenvalues are zero.

For the case of the channel matrix being *unknown* at the transmitter and with the MEGs being equal, it is logical to divide the transmit power (relates directly to SNR) equally between the transmit antenna elements, and this appears in the capacity equation below as the term SNR/N_t.

For the case when the channel matrix is *known* at the transmitter, an optimal link (dirty paper coding) is possible. In this case, singular value decomposition of the channel matrix, $\mathbf{H} = \mathbf{U_r}\Lambda\mathbf{V_t}^+$, gives: the sets of the receiving antenna weights (each of the N_t weight sets being the conjugate of an $(N_r \times 1)$ column vector from the $(N_r \times N_t)$ matrix $\boldsymbol{U}_r$); the corresponding sets of transmit weights (each of the N_r weight sets being a $(1 \times N_t)$ row vector from the $(N_r \times N_t)$ matrix $\mathbf{V}_t^+$); and the corresponding amplitude gains, $\lambda_i = \tilde{\lambda}_i^{1/2}$, of the eigenchannels from the diagonal matrix Λ. Waterfilling can be used to optimally allocate transmission powers to a subset of the eigenchannels.

A pragmatic approach is to deploy only the highest gain eigenchannel. This is because the gains of the eigenchannels (which relate directly to capacity) drop quickly with the increasing number of eigenchannels, so diminishing returns set in quickly, and of course the antenna complexity (if we include the signal combining as part of the antenna) increases for multiple eigenchannels because of the need for multiple sets of weights, etc., at the transmitter and receiver. As an example [13], an ideal 4×4 link has 16 uncorrelated paths, and if all of the eigenvalues could be used in a transmit-diversity or receive-diversity situation, the gain relative to a 1×1 link would be 16 (12dB - which is the same as in a free space situation with no multipath - 16 elements with unity gain), and a diversity order of 16. But this performance is not possible in a single 4×4 eigenchannel because the maximum eigenchannel gain is only about 10dB. The reason for this reduction is because in a 4×4 eigenchannel, there can be a maximum of 8 weights, which is not enough for the 16 channels, i.e., $(4 + 4) < (4 \times 4)$.

For a single-user system with $N_r = N_t$, it turns out that the (single-user) capacity does not change much between the known and unknown cases, although interference to other systems will be increased for the unknown case.

For large-N_t systems whose channels are changing quickly, the required quick-updating of the channel acquisition and its interchange between transmitter and receiver, can dominate the capacity resource, so the point of the MIMO system is lost. Getting around this problem is an ongoing research topic, and so the unknown channel is usually the case of practical interest.

For unknown channels and a large mean SNR in the sense that $(SNR/M_t)\lambda_k >> 1$, the "ergodic" capacity expression simplifies to an SNR term plus a channel richness term:

$$C = log_2\left\{det\left(\mathbf{I}_{N_r} + \frac{SNR}{M_t}\mathbf{HH}^+\right)\right\}$$
$$\approx 0.33N\left(\frac{SNR}{M_t}\right)_{in\ dB} + \sum_{i=1}^{k} log_2\tilde{\lambda}_i, \quad \text{(large SNR)} \quad (8)$$

where the 0.33 is from the log conversion. This form is useful to the antenna designer because it reveals the contributions of the mean SNR, relating to the MEGs, and to the channel richness, governed by the cross-correlations. Non-zero correlations degrade the above capacity as follows. The ideal channel matrix is denoted $\mathbf{H}_w^+$, where subscript w ("white") indicates zero-mean, uncorrelated complex gaussian elements. A correlated channel can be expressed as $\mathbf{H} = \mathbf{R}_r{}^{1/2}\mathbf{H}_w\mathbf{R}_t{}^{1/2}$ where $\mathbf{R}_r$ and $\mathbf{R}_t$ are the correlation coefficient matrices for the receive and transmit antennas. The transmit correlation matrix is taken from its receiving case formulation, ρ, in Section *A* above.

This capacity is a theoretical limit, and it is often called an achievable capacity (or achievable rate) in engineering publications, but "achievable" is a purely mathematical reference. What is achievable in engineering practice can never be very close to this, because of the limitations of practical communications techniques, e.g., [28]. So the value of the capacity is of limited utility as a metric for antenna design unless the degradations from the communications signal processing and

the propagation behaviour are well defined. Nevertheless, it provides a metric to compare antennas, even if we cannot readily interpret the impact of the difference. The capacity (in bits/sec) is also directly proportional to bandwidth, which is normally limited in a system by the antenna. This is especially the case when the antenna operates as a set of differently-behaved embedded elements in multipath. This resulting bandwidth is formulated from the TARC, with an example in Section II.

The capacity formula above can be used as a summation over narrowband channels to evaluate a wideband channel, and OFDM is the usual approach for deploying antenna diversity across a wide bandwidth. The SNR is directly proportional to the antenna system gain, expressed by including the DG with the path gain and other factors of the Friis equation. It is noted that for blindly optimized antenna designs, a design optimized for a capacity can be expected to be different to one optimized for maximum DG, or for maximum mean SNR, etc.

Finally, it is emphasized that the capacity (and correlations, MEGs, and DG, etc.) depend on both the antenna design and the propagation scenario. If the antenna is not reconfigurable, and must work in many scenarios, the design must be derived from an averaged propagation scenario. So, we normally design - and optimize in some sense - for an averaged scenario. It follows that at any specific time for a changing scenario, the antenna design is unlikely to be optimal. While the capacity can be mathematically expressed as an instantaneous metric, it is normally taken from an expectation or averaging, such as using an average propagation scenario. A capacity example is calculated below for the uniform scenario using a commercial package called MIMObit [29].

F. ANTENNA EFFICIENCY (η_{ANT})

Good radiation efficiency is always a focus for antenna design, but it can be hard to achieve with mobile terminals. As a current example, LTE communication systems antennas are expected to provide over 40% - 50% efficiency [30]. The losses from the antenna structure (metals, radome, support materials, etc.), substrate material, matching components, and the platform, all contribute to degrading the radiation efficiency. In a diversity system, mutual coupling can also reduce antenna efficiency. The mechanism is that some of the transmit power of one port goes to other ports instead of directly contributing to the radiation. This is often a dominant design issue because we are normally trying to pack several antennas in close proximity. In general, the antenna efficiency takes a double toll on the SNR - the ohmic loss of the antenna signal firstly attenuates the signal, and secondly, it increases the thermal noise. In most terrestrial communications, the thermal noise is below the interference, and so the impact on the SNR (or rather SNIR) is often simply taken only as the signal attenuation mechanism.

G. ELECTROMAGNETIC ISOLATION (EI)

Electromagnetic isolation [31], sometimes called the structural isolation, is a term for the coupling (here meaning a scattering parameter S_{ij}) when the elements are simultaneously conjugate-matched in order to remove the impact of impedance mismatch. An example in [32] shows how EI can guide the choice of diversity antenna configurations of given elements on a given aperture. When the ports are not matched, S_{ij} is often used as a measure of the isolation, but it does not tell the full story because S_{ij} depends on the reflections, e.g., S_{ii}. An alternative approach is to use a normalized mutual impedance such as the r_{ij} above (or its s-parameter equivalent) to express the mutual coupling.

H. TOTAL ACTIVE REFLECTION COEFFICIENT (TARC)

The Total Active Reflection Coefficient (TARC, Γ_a^t) gives a measure of the degradation of the radiation efficiency of the antenna system caused by the mutual coupling. It is [33]

$$\Gamma_a^t = \sqrt{\frac{avail.\ power - rad.\ power}{avail.\ power}} = \frac{\sqrt{\sum_{i=1}^{N}|b_i|^2}}{\sqrt{\sum_{i=1}^{N}|a_i|^2}} \quad (9)$$

where a_i is the usual incident signal at the antenna port (so this represents the transmit signal) and b_i is the reflected signal, i.e., $[b] = [S_p].[a]$, with $[S_p]$ the usual s-parameter matrix. For lossless antennas and structures, Eq. (9) is convenient for finding efficiency and bandwidth limits directly from the antenna scattering parameters, rather than having to take pattern measurements. For a 2-element diversity system [34],

$$\Gamma_a^t = \sqrt{\left|\left(S_{11} + S_{12}e^{j\theta}\right)\right|^2 + \left|\left(S_{21} + S_{22}e^{j\theta}\right)\right|^2}/\sqrt{(2)} \quad (10)$$

and this is expressed for larger systems in [35].

The TARC is between zero (when all the transmit power is radiated) and one (when all the power is either reflected back or re-enters via other ports). In Eq. (10), θ indicates the phase between the two element signals.

The propagation conditions, or rather their channel characteristics, can be mapped to transmission signal distributions so that we can use Monte-Carlo simulations of the complex amplitude gains, a_i in the TARC expression, for estimating the antenna system efficiency limits. The resulting graphs (see below, for Rayleigh channel signals and using simultaneous signal combining) give a guide for a lossless antenna's worst-case bandwidth owing to the impact of the coupling and the propagation scenario.

I. RELATIONSHIP BETWEEN ECC, η_{ANT} AND DG

Practical, real-world elements are lossy, and have mutual coupling and associated non-zero correlations. The DG is the diversity performance metric, but its dependency on the differences between the MEGs, and the correlations, can be cryptic. The designer must get a feel for the performance tradeoffs of the antenna system design choices. For example, Fig. 1 depicts the MRC-DG for a

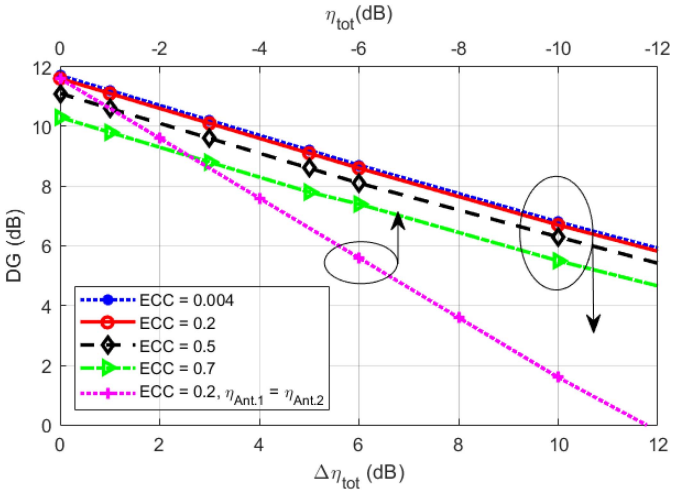

FIGURE 1. Relationship between performance (DG), and efficiency, branch MEG imbalance, and ECC, for a two-port antenna in a uniform scenario.

two-port antenna for a range of ECC, with loss expressed as antenna efficiency (η_{ant}), and MEG ratio as the difference efficiency $\Delta\eta_{ant}$ in dB. The DG is calculated using equation (7). In general, a scaled correlation matrix is first calculated using the product of square matrices, $\boldsymbol{\rho}_{scaled} = \boldsymbol{\eta}_{tot}^{1/2}\boldsymbol{\rho}_{unscaled}\boldsymbol{\eta}_{tot}^{1/2}$, where the diagonal matrix $\boldsymbol{\eta_{tot}}$ contains the antenna element total efficiencies. When the efficiencies are all the same, the scalar multiplier is just $\boldsymbol{\rho}_{scaled} = \eta_{tot}\boldsymbol{\rho}_{unscaled}$.

The left vertical axis of Fig. 1 represents the ideal situation of unity antenna efficiencies. While this is just for two antennas, the same basic tradeoffs hold for higher order systems.

In the following sections, examples are presented, applying the above metrics for design and evaluation.

III. DIVERSITY SYSTEM EVALUATION BENCHMARKING

This section presents diversity evaluation of "generic" antennas, which can be used as standard antennas for developers to use to benchmark their own, and in-house, evaluation processes. In [11], correlation evaluation benchmarking uses an analytic solution for the pattern of a special testing antenna. But for nearly all IoT device antennas, no such analytic model is accurate for the pattern, especially PCB-based ones. Our measurements are from two different professional facilities labelled SFU for our laboratory system, and SW for the facility at Sierra Wireless Inc. Such a comparison has not been reported before as far as we are aware, but because of the complexity of pattern measurement, the comparison is important for understanding the repeatability accuracy. The simulations use CST Microwave Studio [36]. The benchmark designs are depicted in a selection of the figures below with part (a) showing the structure and part (b) the various ECCs. The simulated and measured results from s-parameters, and from pattern inner products, are denoted $\text{ECC}_s^{(sim)}$, $\text{ECC}_s^{(meas)}$, $\text{ECC}_{ip}^{(sim)}$, $\text{ECC}_{ip}^{(meas)}$.

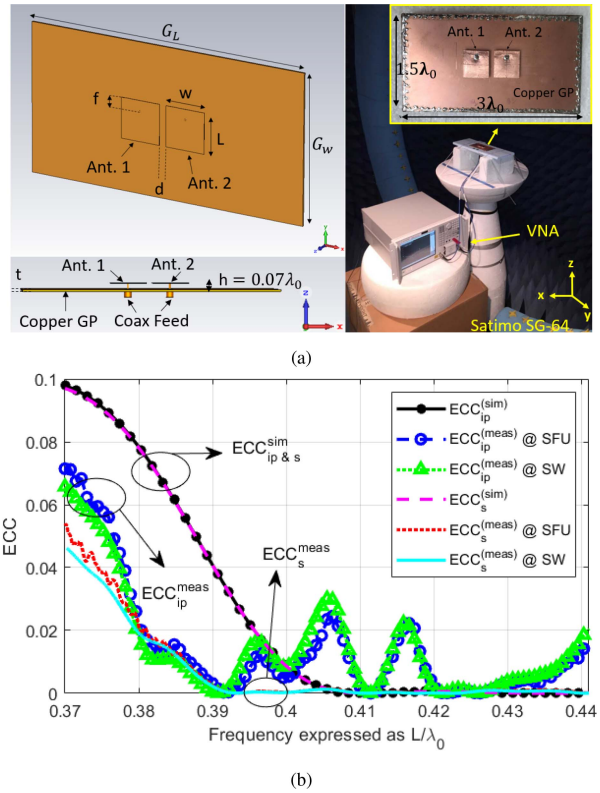

FIGURE 2. Benchmark #1: (a) dual air-substrate copper patch antennas (i.e., low loss at microwave frequencies) with $G_L = 3\lambda_0$, $G_W = 1.5\lambda_0$, $W = 0.43\lambda_0$, $L = 0.42\lambda_0$, feed position $f = 0.07\lambda_0$, $d = 0.07\lambda_0$ and air-substrate thickness $0.07\lambda_0$, @ 5.75GHz. (b) ECC, by simulation and by measurement calculated from s-parameters and pattern inner product from measurements at two independent facilities. The measured ECCs demonstrate excellent repeatability, and are different between the s-parameter and pattern formulations. The pair of simulated results agree with each other as expected, and are different to the measured results.

A. DIVERSITY PATCH ANTENNAS

1) EFFECT OF LOSS (BENCHMARKS #1 AND #2)

Figure 2(a) presents an all-metal, dual patch diversity system (benchmark #1). The metal is copper, so this structure is almost lossless at microwave frequencies, and has a total efficiency of about -0.17dB.

From Section II, it is of particular interest to see the similarities and differences for the various ECC calculations for a practical, almost-lossless structure, and this is in Fig. 2(b). The simulation results from the s-parameters and from the patterns, $\text{ECC}_s^{(sim)}$ and $\text{ECC}_{ip}^{(sim)}$, match, as can be expected from an almost-lossless structure. The measured pattern results, $\text{ECC}_{ip}^{(meas)}$, from the two facilities are very close to each other, demonstrating the level of repeatability of the pattern measurement approach, at least when using professional-level facilities. The measured s-parameter results, $\text{ECC}_s^{(meas)}$, from the two facilities, also match each other, confirming repeatability of the "open air" VNA measurements, although this is a less demanding measurement than patterns.

There is a significant difference between the measured and simulated results. This is because they are for different structures in the sense that the simulation one is an

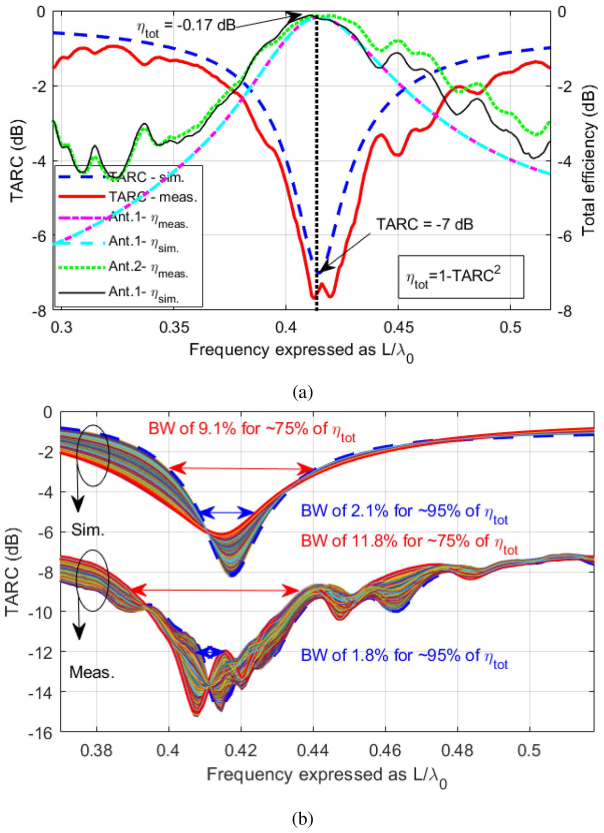

FIGURE 3. **(a) Total efficiency and TARC for benchmark #1 with $\theta = 0°$ when one port is excited and the other loaded with 50Ω, (b) TARC calculated using simulated and measured s-parameters of #1, with both ports excited with random Rayleighs. The lower plot has an offset −6dB for display convenience. This use of TARC gives the bandwidths for a given radiation efficiency for a multiport antenna operating in dense multipath.**

ideal configuration and construction, and the measured one is hand-constructed and has a feed cable configured in a real-world way (imperfectly positioned, etc.).

It is important for designers to have a feel for the typical size of this difference in the ECCs, and this example (Fig. 2(b)), plus those below, establish typical differences. The simulated results from the patterns and the s-parameters coinicide, as expected from a low-loss structure. The measured results are different to the simulated ones. The measurements have excellent repeatability - both the s-parameter- and pattern-derived results are very similar for both measurement facilities. But the ECC from measured s-parameters and measured patterns are different from each other - the $\text{ECC}_{ip}^{(meas)}$ features ripples with frequency, whereas the $\text{ECC}_{s}^{(meas)}$ falls monotonically and stays at essentially zero. The size of this difference is typical and is due to the structural differences between the simulated model and the measurement prototype, in particular including its feed system and cable which is often not modelled in simulation. Although the relative error between the correlations is high, the absolute error is low - the maximum difference due to the ripples is only about 0.03 (relative to the unity scale of the coefficient). As noted in Section II, the angular sampling density is not a factor in the accuracy of these calculations.

For lossless antennas, and in practical low-loss structures, the TARC provides a revealing measure of the multiport antenna efficiency. Figure 3(a) shows for benchmark #1, the simulated and the measured TARC values (left ordinate) and total antenna efficiencies (right ordinate), for simulations and measurements. The measured TARC is about 1dB below the simulated one, again because we have somewhat different structure detail, and this difference value (i.e., about 1dB) indicates a typical margin that can be expected by designers from a hand-fabricated PCB antenna and the presence of cables in the measurement of it. For example, from simulation, using the s-parameters or the pattern inner product, the total efficiency at 5.6GHz (peak of the curve, labelled with a vertical line in Fig. 3(a)) is about −0.17dB, and this is the same as that calculated from the TARC expression. From measurement, the total efficiency is ∼−0.14dB, calculated from either the s-parameters or the TARC; however, the total efficiency calculated via the pattern inner product is ∼−0.6dB. This difference indicates the typical impact of simulation-vs-measurement on this metric, when there is good accuracy in the pattern measurement. Figure 3(b) shows the TARC for Rayleigh channels (Rayleigh distributed amplitudes and uniformly distributed phases for the narrowband channel signal). This is very informative and the first such calculation using Rayleigh channels as far as the authors are aware. The lower plot is shifted down by 6dB for display convenience. For maximum TARC values of ∼75% (for a −3dB TARC bandwidth) and ∼95% (−6dB TARC bandwidth), the bandwidths are respectively about 11.8% and 1.8% from measurement (see, 9.1% and 2.1% from simulation). These numbers offer typical variations for this benchmark, but the method can be used for any multiport antenna. They show how much the usable bandwidth reduces when considering the simultaneous combining of MIMO applications (such as using space-time coding), in a typical PCB based antenna. Different distributions, such as Rician, etc., can be used for different propagation conditions.

The −3dB and −6dB impedance bandwidths (calculated from the s-parameter behaviour, not shown here) are about 29% and 12.4% for measurement, and about 18% and 11.1% for simulation, respectively.

This completes the TARC discussion and we now address the ECC. To clear the way, an intriguing point is that the ECC formula using impedance s-parameters for lossless antennas [15], [16] shows that when the elements are perfectly matched (i.e., $S_{11}, S_{22} = 0$) then the ECC goes to zero, i.e., the patterns become orthogonalized in the uniform scenario and the mutual resistance is zero. (The antenna designer needs only to match the antennas.) This has not been demonstrated before, so we show this by simulation. Figure 4 demonstrates that the ECC indeed becomes zero for matched ports, showing that the matching orthogonalizes the patterns of the embedded elements. The plot in Fig. 4 is for benchmark #1 (Fig. 2(a)), and the approach offers a

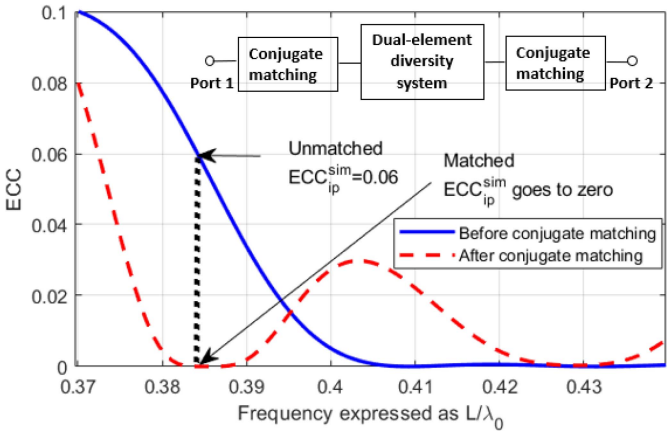

FIGURE 4. ECC calculation from simulated pattern inner product of a lossless diversity antenna, before and after conjugate matching of both ports, for a uniform 3D scenario. The matched ports force orthogonal patterns over the uniform multipath propagation distribution.

helpful check that a diversity evaluation procedure is making sense.

Our second benchmark antenna is another dual patch system (benchmark #2, see Fig. 5(a)) which is similar to benchmark #1 but has lossy FR4 substrate with $\epsilon_r = 4.3$, $\tan\delta = 0.025$ and thickness of 0.8mm ($0.01\lambda_0$ @ 5.75GHz). This type of FR4 substrate has been used for the other PCB antennas below. The effect of loss is of particular interest in diversity evaluation since some of the metrics are based on zero loss antennas. The radiation efficiency is about 55% in simulation (59% in measurement), but plots of these details are omitted for brevity. The particular interest is the EEC - the differences between the simulated and the measured ECCs from the s-parameters, and patterns, see Fig. 5(b).

The ECCs from the s-parameters and patterns, from simulation, do not match well, as expected for a lossy structure (since the s-parameter formulation relies on lossless antennas). The margin indicates the inaccuracy of the s-parameter approach for a typical PCB antenna ECC estimation. This limitation of the s-parameter formulation makes its hard to be used for real antenna design. The measured ECC from patterns, from both facilities, match well, again indicating good repeatability. They are different from the simulation-based results, due to prototyping inaccuracy (dimensional differences, including the feed point location, and the presence and orientation of the feed cable in measurements) and also different substrate permittivity values where we had to use some guesswork. (It is known that the permittivity can change between different batches or between different manufacturers.)

In the following, the effect on diversity performance of loss in the antenna and separately in the feed (not part of the antenna in an antenna-theoretic sense) is investigated.

As noted above, the s-parameter-derived ECCs assume a lossless structure. This leads to differences between the ECC calculated from s-parameters and calculated from patterns, in both simulation and measurement, e.g., [32]. The pattern-derived ECC values for different values of substrate loss

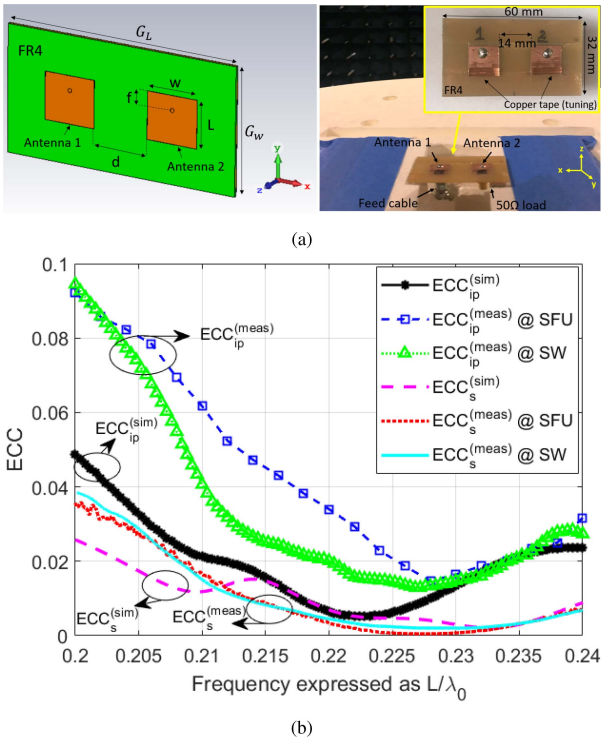

FIGURE 5. (a) Benchmark #2: dual lossy diversity patch antennas with groundplane length $G_L = 1.1\lambda_0$, groundplane width $G_W = 0.61\lambda_0$, patch width $W = 0.25\lambda_0$, patch length $L = 0.23\lambda_0$, feed position $f = 0.07\lambda_0$, antenna spacing $d = 0.26\lambda_0$ and FR4 substrate thickness of $0.01\lambda_0$ @ 5.75GHz. (b) ECC against frequency (electrical length of patch), calculated from simulation (pattern inner product and s-parameters), and also from measurements at independent facilities, showing typical repeatability accuracy, and typical difference from simulation results.

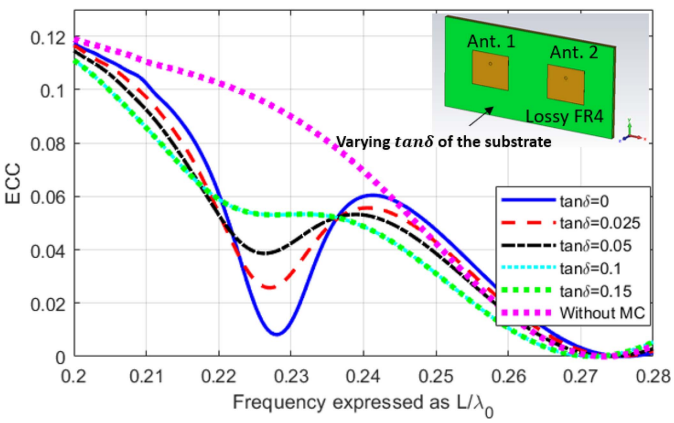

FIGURE 6. Simulated ECC calculated from pattern inner product for different loss values ($\tan\delta$) for the FR4-type substrate of benchmark #2, against frequency (electrical length of the patch).

($\tan\delta = 0$ to $\tan\delta = 0.15$) for benchmark #2 are shown in Fig. 6. The curve "without mutual coupling" represents the case when each element is considered in the absence of the other, and the ECC was calculated from their isolated patterns. The curves show how the ECC decreases with frequency, i.e., as the electrical spacing between the elements increases, for this class of antenna. With the mutual coupling included, the embedded element patterns become different

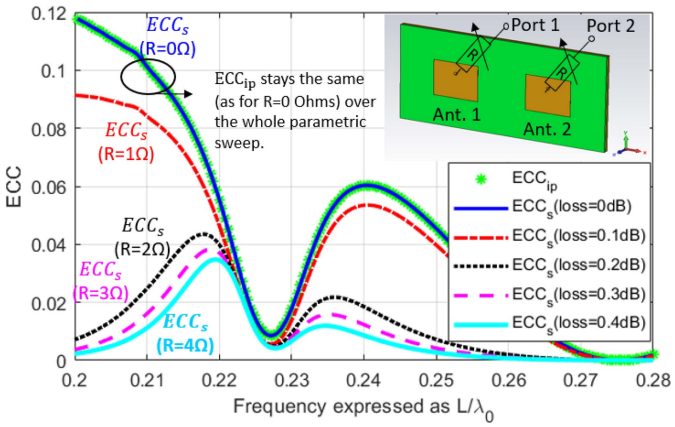

FIGURE 7. Simulated ECC calculated from pattern inner product, and s-parameters, for different loss in the external components of benchmark #2 with lossless substrate.

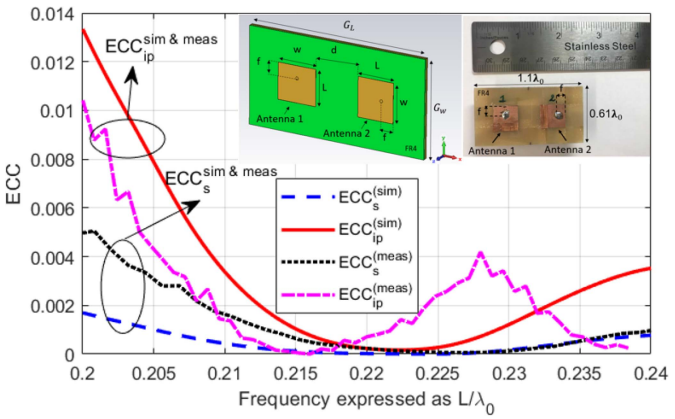

FIGURE 8. Benchmark #3: ECC from simulation and measurement, calculated using the pattern inner product, and the s-parameters, the antenna is the same as benchmark #2 but with one of the patches rotated by 90°. These differences represent, for this type of antenna, typical uncertainty for this metric from using different estimation approaches.

to their isolated patterns. The mutual coupling affects the feedpoint impedance as well of course. In Fig. 4, we have shown how matching the antennas forces the ECC to zero, or at least to a very low value. For benchmark #2, it was observed (not shown here for brevity) that increasing the substrate loss deteriorates antenna input match and improves isolation at the same time, as expected. This is why, in Fig. 6, the ECC goes from a low value (for $\tan\delta = 0$) to approach the no-mutual coupling (isolated elements) case. Figure 6 also indicates that varying the substrate loss of this structure shifts the ECC results only slightly. Figure 7 shows how *external* losses including the loss in matching components or the measurement cables, affect the s-parameter derived ECC. The pattern-derived ECCs stay together for the whole parametric sweep range, confirming that the patterns stay the same when varying just the external losses. This demonstrates that the ECC from (embedded) patterns is accurate, including when there are losses. The s-parameter approach gives optimistic (too low) correlation results for lossy antennas.

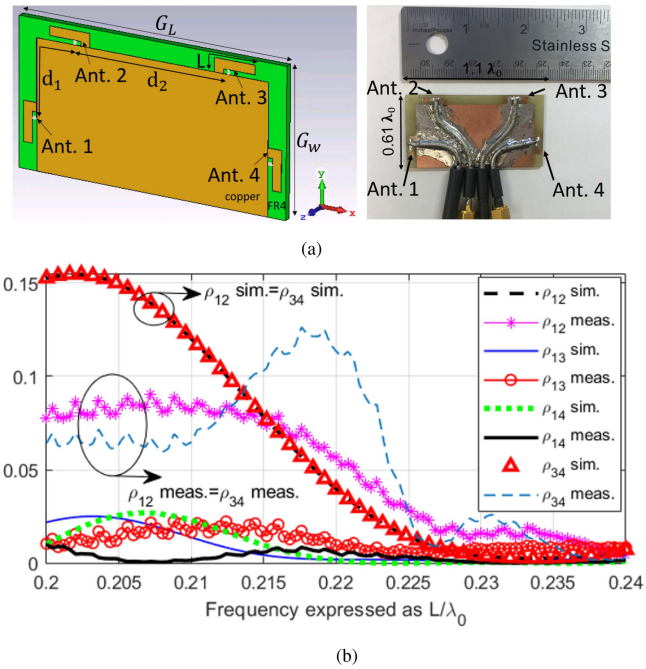

FIGURE 9. (a) Benchmark #4: four PIFA antennas in a generic PCB layout with groundplane length $G_L = 1.1\lambda_0$, groundplane width $G_W = 0.61\lambda_0$, $d_1 = 0.49\lambda_0$, $d_2 = 0.66\lambda_0$ and $L = 0.24\lambda_0$. (b) ECC calculated from simulated and measured patterns. The corresponding pairs, 1-2 and 3-4, ideally have the same correlation (seen in the simulation results), and the ECC differences between these pairs indicates the typical uncertainty from a measurement and using a hand-built prototype.

2) EFFECT OF DIVERSITY TYPE (BENCHMARK #3)

This section shows the effect of diversity type (i.e., the mechanism used to decorrelate patterns) on a diversity/MIMO system. Polarization diversity is deployed in addition to the existing space diversity, in this case by rotating one of the patches by 90^o. This is benchmark #3.

The ECCs from the s-parameter and the pattern approaches are shown in Fig. 8. The agreement between simulated and measured results of benchmark #3 is better than that of benchmark #2, again giving a feel for how typical hand-prototyping inaccuracy changes the ECC in this type of antenna. The closer agreement is in part because the rotated patches have more isolation and so there is a reduced influence of prototyping inaccuracy in one element affecting the other. Note that the impact of the rotation (here for a uniform scenario) brings the ECCs down by a factor of almost 10.

B. PCB IOT DIVERSITY PIFAS (BENCHMARK #4)

Chassis-mounted Inverted F Antennas (IFAs) are another class of PCB antenna which are often used for cellphone and IoT terminals. In [37], the diversity performance of different configurations of a pair of IFAs was studied. The IFAs on a PCB are normally mounted in the corners of a rectangular chassis, but in [37], we include a pair of colinear IFAs on the long edge as well in order to investigate the impact of spacing only, i.e., without any rotation which brings in

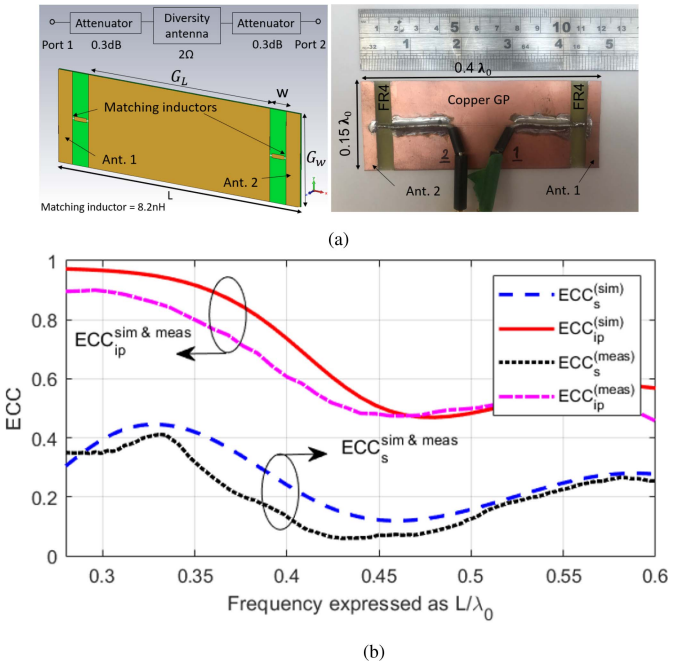

FIGURE 10. (a) Benchmark #5: capacitively coupled dual elements with groundplane length $G_L = 0.3\lambda_0$, groundplane width $G_W = 0.15\lambda_0$, $W = 0.02\lambda_0$ and $L = 0.4\lambda_0$. (b) ECC from measured and simulated s-parameters and from patterns. For these large correlations and a lossy antenna, the s-parameter and the pattern results are very different.

polarization diversity. Based on that study, a four-IFA configuration is shown in Fig. 9(a). This is benchmark #4. The ECCs presented in Fig. 9(b) align with those in [37]. The measured and simulated ECCs are different but these are relatively small differences compared to those typically caused by hand-prototyping, and by measurement cable effect [38] which was not included in the simulations.

C. CAPACITIVE COUPLED ELEMENTS (BENCHMARK #5)

The above benchmarking examples have small ECC values (0.1 or less) because the elements are well separated, and the structures are electrically big enough to support different radiation modes. In practice this is not always the case and smaller structures bring increased correlation and reduced efficiency. In this subsection we will investigate one such diversity configuration popular in mobile communications devices - capacitive coupled elements [39], shown in Fig. 10(a). This is benchmark #5. As the largest dimension (L) is about half-wavelength (at 1GHz) the single radiation mode of the device chassis must be shared between the ports. In the numerical model an attenuator was added to each antenna port to account for the losses in measurement cables. Also, a suitable resistor (2Ω) was added to each inductor (8.2nH) to include the effect of matching component loss. These are shown in the block diagram in Fig. 10(a). The ECCs shown in Fig. 10(b), are typical for this class of antenna, showing how different the ECCs can be between the s-parameter- and pattern-formulations.

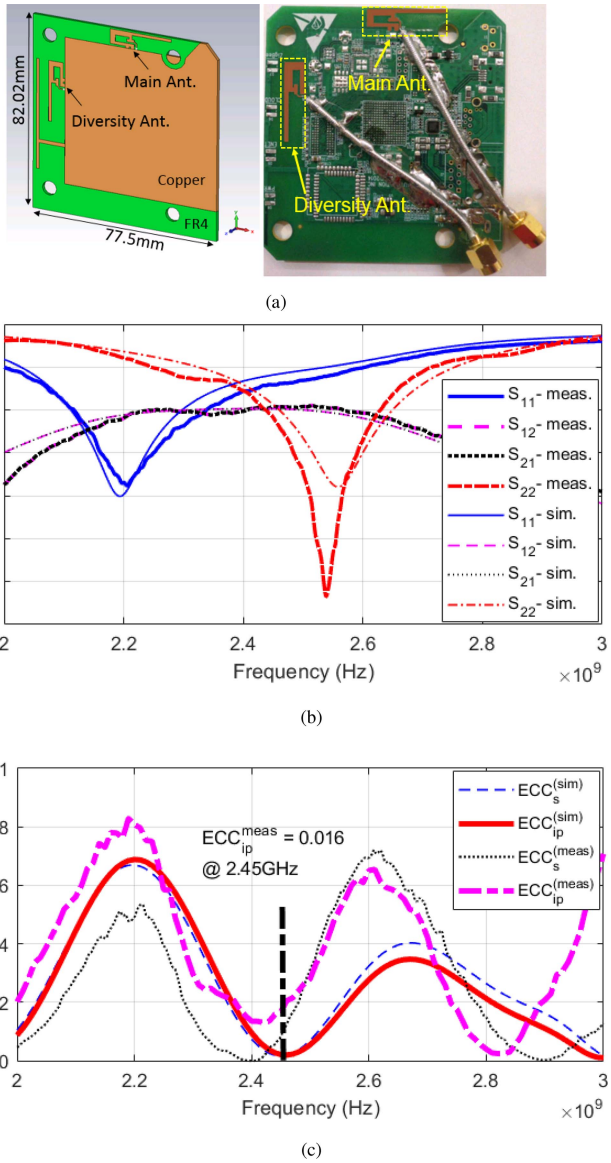

FIGURE 11. (a) A typical PCB IoT device, by Rainforest, with diversity antennas spaced and rotated by using different edges of the board, (b) simulated and measured s-parameters showing the tuning at different frequencies. (c) ECC from simulated and measured s-parameters and patterns for a uniform propagation scenario.

IV. IMPACT OF POLARIZED SCENARIO ON A TYPICAL PCB IOT DIVERSITY ANTENNA

A. ELEMENTS WITH SPACE AND POLARIZATION DIVERSITY

This section demonstrates the impact of a polarized scenario on the performance of a typical PCB-based IoT device, specifically on its MEG and its capacity distribution. The PCB example product is manufactured by Rainforest Automation Inc., and the testing prototype is shown in Fig. 11(a). The IFA antennas are spaced and rotated, i.e., two different pattern decorrelation mechanisms are deployed. The patterns indeed have very low correlations in the uniform scenario, shown below, but the diversity performance of the device can still be vulnerable to the polarization of the propagation, also demonstrated below. The basic s-parameters plot

is in Fig. 11(b). The elements are tuned to spaced frequencies because this design was also to investigate frequency diversity (spaced frequencies normally using the same antenna, results below in Fig. 14), but where the two frequencies use different antennas for electronic hardware convenience. Here we simply deploy them as diversity antennas, operating at a frequency (2.45GHz) which is between the tuned frequencies, and accept the mismatch (the S_{11} and the S_{22} are still less than -6dB). The isolation (here as S_{12}, S_{21}) measurement is about -10dB across all the frequencies of interest. The simulated ECCs, in Fig. 11(c), calculated from s-parameters and patterns, are in reasonable agreement. The measured results are somewhat different to the simulation results, and from each other (i.e., the pattern- and s-parameter based formulations), as the frequency increases. While the relative difference is large, the absolute difference is small, with the full scale of the abscissa being only 8% of the positive correlation coefficient range. The important information, in the context of this article, is that these variations between simulation and measurement, and between measured s-parameter- and pattern-based calculation, are typical for hand-built prototypes, and as noted above, repeatable. There is further comment below (Fig. 14) regarding patterns for this type of PCB antenna.

Figures 12(a) and 12(b) show the Rainforest PCB mounted horizontally and vertically in a Satimo near field pattern measurement chamber, with its two antennas magnified in the photo inserts. From these measurements, and using a polarized uniform scenario model, Fig. 12(c) emphasizes how the MEGs (and therefore DG) is sensitive to propagation parameters and device orientation. In the worst case polarization scenario on this plot (rhs of the plot; θ polarization, horizontal mounting), the MEGs are around -9dB and -10dB, and the best case (top left of plot) about -4 and -5dB. These results include the impedance mismatches, so strictly the metric should be referred to as a "total MEG". The worst case difference between MEGs on this plot is about 2dB. From Fig. 1, with a low ECC, this MEG imbalance of 2 dB reduces the MRC-DG by about 1dB. It was shown in [40] that as a result of adding the diversity branch, the SNR-outage probability can be expected to improve from 15% to 2%.

The capacity, following Section II, expressed as its cumulative distribution, is in Fig. 13.

The capacity is a function of the SNR and antenna metrics, as discussed above, and expresses the antenna parameters - MEGs and ECCs, in terms that can be used by communications system designers. The figure shows the increase in capacity for the diversity system compared to that of using a single antenna, for a given average SNR. Here, for demonstration, we used an average SNR of 50dB, which is higher than most real-world systems. This calculation, from equation (7), was from software called MIMObit [29], and is here for a polarized uniform scenario. This capacity gives a potential communications capability comparison for the Rainforest two-antenna diversity system against the single

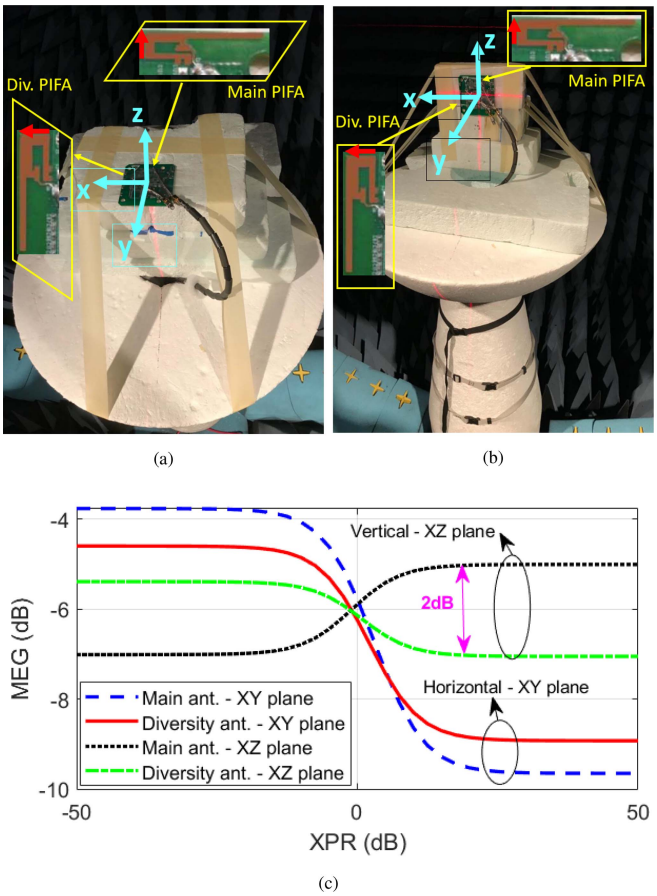

FIGURE 12. Pattern measurements of the Rainforest IoT device in a Satimo SG-64 anechoic chamber with (a) horizontal (xy plane) mounting orientation and (b) vertical (xz plane) mounting orientation, (c) The total MEG calculated for the Rainforest IoT device in a uniform distribution for each polarization but with a varying ratio of powers in each polarization. The ϕ polarization is to the left and the θ polarization is to the right. When the XPR is 0dB (equal power in each polarization), the MEG is half the radiation efficiency, independent of the pattern, and here, with total MEGs of -5.76dB and -6.26dB, and mismatch gains of -1.25dB, the radiation efficiencies follow as about -1.5dB and -2.0dB.

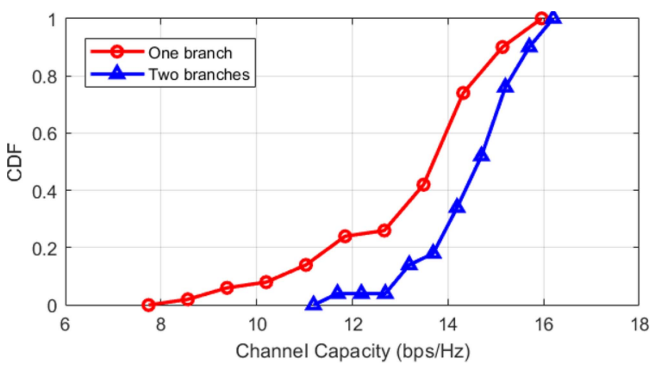

FIGURE 13. Capacity for Rainforest board (uniform 3D propagation scenario), using commercial software [29].

antenna solution. For example, for a 10% capacity outage (CDF = 0.1), the improvement in capacity is ~2 bits/sec/Hz.

As an alternative to spatial and polarization diversity, frequency diversity can be studied using the PFCF to indicate the minimum carrier frequency shift required for diversity

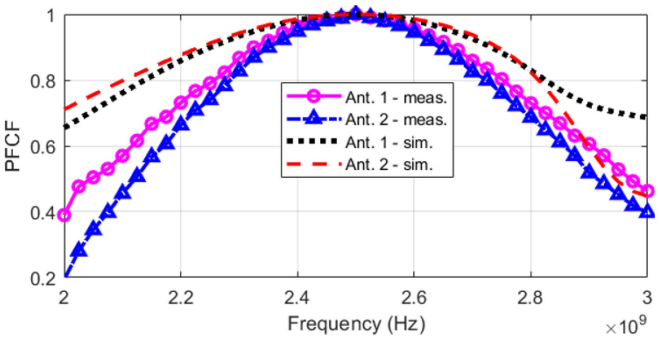

FIGURE 14. PFCF from measured and simulated patterns for Rainforest board.

action for a given antenna. The simulated and the measured PFCFs for this example are presented in Fig. 14 for the uniform scenario. The PFCF for the measured patterns drops quicker than that of the simulated ones. This is due extra scattering from the electronic components on the PCB creating more complex patterns, with the componentry not being part of the simulation model. Here the carrier frequency is centred at 2.45GHz, and, for example, the 0.7 correlation bandwidth for simulated and measured patterns is ∼0.45GHz, and ∼0.3GHz, respectively. So, from the measured patterns we need a minimum frequency spacing for this antenna of about 0.3GHz for frequency diversity. This approach provides useful design knowledge for IoT PCB devices. The configuration in Fig. 11(a) has a sufficiently wide bandwidth (requires about a −6dB bandwidth definition) on either antenna and so these would be suitable for frequency diversity.

B. DAUGHTER BOARD ANTENNA FOR POLARIZATION DIVERSITY

Sometimes, it is required to upgrade performance of an IoT device by adding a diversity branch without otherwise changing the existing PCB configuration. (Such an configuration change is an expensive redesign.) Figure 15(a) shows one way forward by deploying a novel daughter-board antenna to support a diversity element which is essentially collocated with the standard antenna pair printed on the PCB. It offers a third polarization component ($\hat{z}$) to the existing orthogonal pair printed on the board ($\hat{x}$ and $\hat{y}$).

The s-parameter plot is in Fig. 15(b), showing bandwidths and the isolation (as S_{ij}) of the co-located ports from simulation and experiment, and their typical alignment. The dimensional inaccuracies of the prototype, differences in dielectric properties of the actual substrate to that used in the numerical simulation (ϵ_r= 4.1, tan δ= 0.035 at 2.45GHz), and the influence of test cables, are the causes of imperfect agreement. Ferrite beads were used (see Fig. 15(a)) to suppress return currents on the feed cable of the daughter board element instead of a proper, but bulky, balun transition; and this reduces, but still contributes, to the cable effect. Also, for this type of antenna, asymmetry in the (hand-) placement of the daughter board element relative to the main PCB,

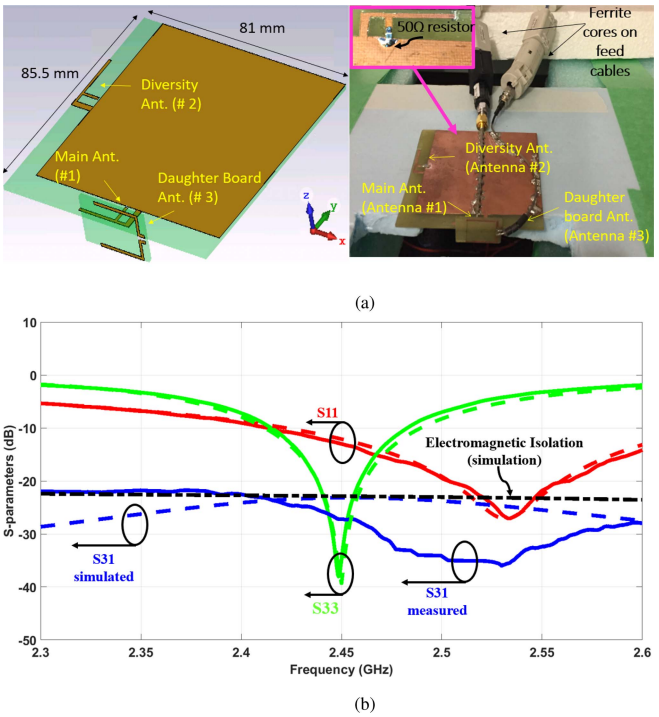

FIGURE 15. (a) On-PCB PIFA and daughter board antennas, (b) s-parameters for the co-located antennas of the daughter board design showing impedance bandwidths and isolation. Only Antenna1 and Antenna3 were considered in measurements, with Antenna2 terminated in 50Ω.

causes variations. The isolation (S_{31}) between the daughterboard antenna (Antenna3) and Antenna1 is better than −20dB. Antenna structures with such inherently high isolation are easier to design in the sense that one element can be tuned independently of the other. The patterns are in Fig. 16 (simulated) and Fig. 17 (measured) showing typical similarity for PCB antennas. While the pattern of Antenna3 looks like a vertical dipole (the dipole-like source corresponds to the feed orientation of the antenna) in its horizontal cut, it also features an omni-like pattern in the $\phi = 0$ cut, and high cross-polarization in its $\phi = \pi/2$ cut. This bodes badly for seeking high polarization purity but is not a barrier for polarization diversity. In summary, the IFAs and the daughter board IFA-pair tend to radiate like dipoles oriented in the direction of their feed, but there is significant cross-polarization compared to a dipole and other pattern distortion from the presence of the PCB.

The ECCs are in Fig. 18 and are very low as expected from polarization diversity and a uniform scenario (i.e., with assumed uncorrelated polarizations in the propagation). A second such daughter board antenna could be placed with the other PCB antenna to give a total of four antennas on the PCB. This daughter board concept is simple, practical, and can add antenna elements in a compact manner.

V. IMPACT OF DIRECTIONAL PROPAGATION SCENARIO ON PCB DIVERSITY ANTENNA PERFORMANCE

In this section, the effect of a directional propagation scenario on diversity performance is studied. Previous works, such

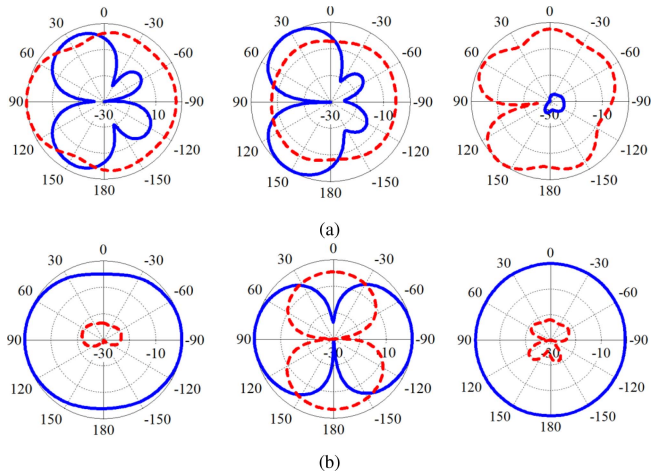

FIGURE 16. Simulated (CST) pattern cuts for the θ- (solid line) and ϕ- (dottedline) polarizations for (a) PCB antenna (Antenna1), and (b) daughter board antenna (Antenna3). Left: (θ, ϕ=0). Middle: (θ, $\phi = \pi/2$). Right: ($\theta = \pi/2$, ϕ) at 2.45GHz.

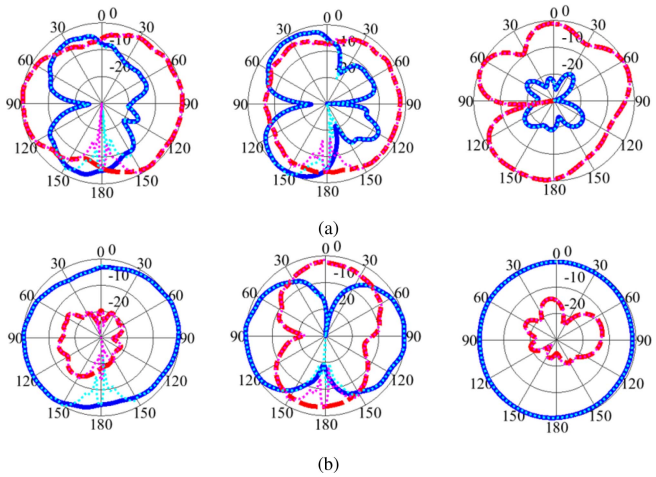

FIGURE 17. Measured (Satimo SG64) pattern cuts for the θ- (solid line) and ϕ- (dotted line) polarizations for (a) PCB antenna (Antenna1), and (b) daughter board antenna (Antenna3). Left: (θ, $\phi = 0$). Middle: (θ, $\phi = \pi/2$). Right:($\theta = \pi/2$, ϕ) at 2.45GHz.

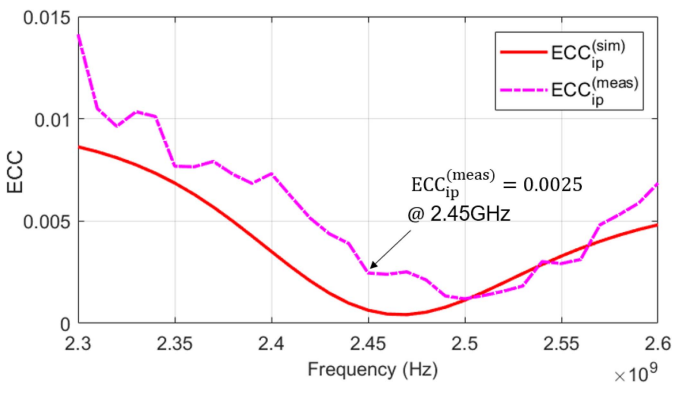

FIGURE 18. ECC from simulated and measured pattern inner product.

as [41], [42] tend to explore directionality in just one dimension. The von Mises-Fisher (vMF) probability distribution function can model directionality in circular coordinates.

TABLE 1. Diversity performance of a typical PCB IoT antenna (Section IV-A) @ 2.45GHz, with MRC combining, in various propagation scenarios.

Simulated Div. Evaluation Metrics	3D Uniform	vMF (XPR = 0dB, $\theta_{mean} = 90°$, $\phi_{mean} = 0°$, $HPBW$ = 90°)	vMF (XPR = 0dB, $\theta_{mean} = 90°$, $\phi_{mean} = 0°$, $HPBW$ = 10°)
ECC (pattern)	0.016	0.1614	0.8299
ECC (S-param.)	0.008	Not Applicable	Not Applicable
MEG1, MEG2(dB)	-5.8, -6.1	-3.51, -7.54	0.74, 3.2
DG(dB)	8.4	8.8	10.3

The pdf for the d-dimensional unit vector X is

$$p(X; \mu, \kappa) = C_d(\kappa) exp\Big(\kappa \mu^T X\Big) \tag{11}$$

where vector μ contains the pattern maximum direction in (θ, ϕ), κ controls the spread or directionality of the distribution, related to the HPBW of the directional propagation, used below, and C_d is for the normalization,

$$C_d(\kappa) = \frac{\kappa^{d/2-1}}{(2\pi)^{d/2} I_{d/2-1}(\kappa)} \tag{12}$$

where I_n is the modified Bessel function of the first kind and order n. For the 3D-vMF (i.e., θ and ϕ directions), $d = 3$.

The ECCs for the Rainforest PCB antennas using the vMF distribution are shown in Fig. 19. The HPBW of the propagation is varying from a small angular spread to the full sphere. The plots show how the increasing directionality of the propagation (decreasing HPBW) increase the ECC values. This approach shows the power of the pattern inner product approach for evaluating the antenna performance, and thereby its communications performance, see [37]. Figures 20 and 21 show the ECC variations for changes in other propagation parameters while keeping the propagation directionality fixed with a HPBW of 90 degrees. This is modelling an indoor scenario where the signal arrives through a window in a room. Whereas we showed above the impact of polarized propagation, here the envelopes of the EEC in Figures 19 to 21 show the impact of propagation directionality and the associated device orientation. This is a very convenient approach to performance evaluation for varying propagation conditions, including the impact of device orientation. Recall that the pattern formulation must be used here (the s-parameter formulation is only for the uniform scenario), and that in using (far-field) patterns, the multipath scatterers of the VMF distribution must be in the far-field of the antenna. Table 1 summarizes performance of the Rainforest board in terms of the main diversity evaluation metrics. It reiterates the observation (in Fig. 1) that the ECC value, as long as it is not large, has less effect on DG than the MEGs and their imbalance. This is for small diversity systems, but with large (many antenna) systems, the ECC becomes critical, and even small non-zero values can have a large impact on the capacity [43].

Figure 22 shows the cumulative densities of the ECCs for a selection of different diversity systems: the Rainforest IoT

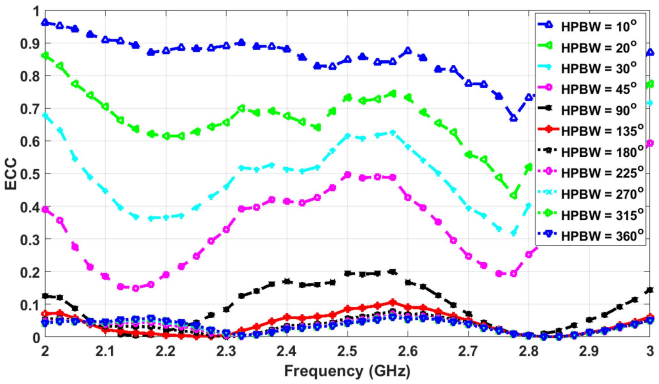

FIGURE 19. ECC for different HPBW for von Mises-Fisher with XPR = 0dB, $\theta mean = 90°$ and $\phi mean = 0°$.

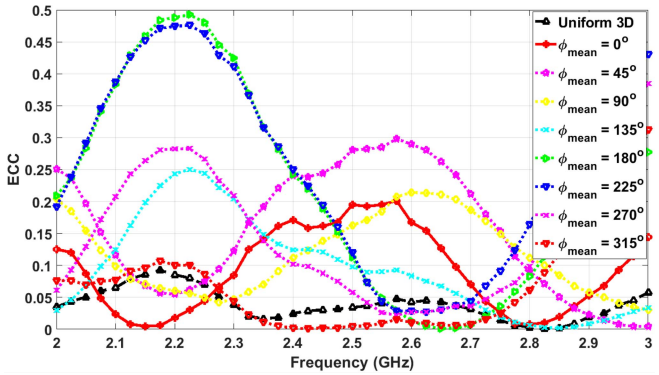

FIGURE 20. ECC for different $\phi mean$ for von Mises-Fisher with XPR = 0dB, HPBW= 90° and $\theta mean = 90°$.

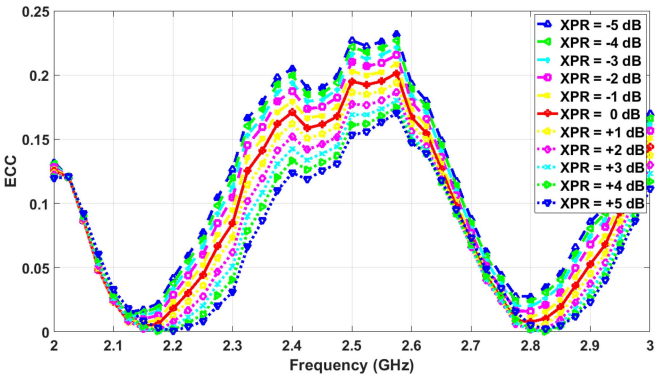

FIGURE 21. ECC for different XPR values, HPBW= 90°, $\theta mean = 90°$ and $\phi mean = 0°$.

board; the daughter board configuration of Fig. 15(a); the capacitive coupled elements of benchmark #5; and canonical antennas - a pair of lossless, crossed and parallel dipoles. For these plots, the propagation scenario is varied - the mean direction of arrival of signals (μ) varies in θ and ϕ, XPR varies from -50dB to $+50$dB (polarization swinging from horizontal polarization to vertical), and the HPBW of the propagation varies from 10 degrees (highly directional) to 360 degrees (almost uniform). The figure shows that for the Rainforest board, the ECC stays below 0.1 for $\sim$80% of the time, whereas for benchmark #5, the ECC is greater than

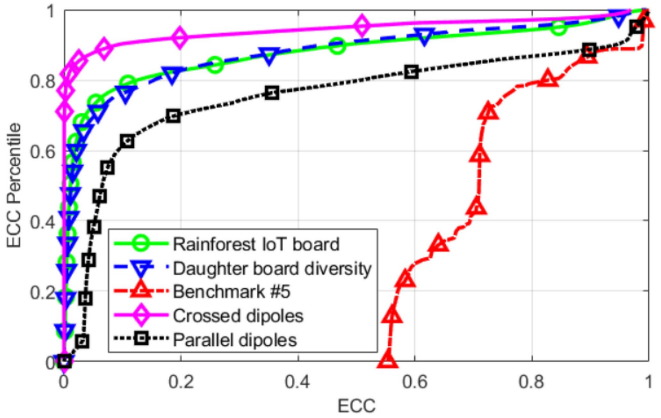

FIGURE 22. CDF of the ECCs for multiple antenna designs, for variations in propagation scenario and the device orientation.

0.5. The canonical example of the crossed dipoles shows the lowest ECC among these systems. Such a canonical model allows designers to have a target ECC to aim for in their designs.

In summary, the correlations and the MEGs govern the antenna performance. Their impact can be presented as communications metrics such as capacity, or diversity metrics such as DG.

The procedure can be extended to study more complex statistical properties of MEG and DG in directional environments that are of interest in practical diversity/MIMO design.

VI. CONCLUSION

Developers of diversity/MIMO antennas require an understanding of many signal-processing based performance metrics, and also require access to a set results to benchmark their in-house evaluation processes. This article contributes to both of these requirements. We reviewed the metrics, clarifying their assumptions and formulations, and presented examples of them derived from both simulation and from physical measurements for a set of PCB-based antennas, including a new polarization-diversity design. Comparisons are included between the correlation results from multiport parameters, and from pattern estimates taken at independent facilities. Antenna loss and feed loss are separately included, as well as the performance impact of polarized scenarios and 3D directional scenarios using the von Mises-Fisher distribution. These results help developers to check the expected accuracy of their evaluation processes comprising both complex measurements and calculations of signal-processing diversity metrics.

REFERENCES

[1] R. S. Brar, R. G. Vaughan, and M. Felipe, "Phased arrays and MIMO: Wideband 5G end fire elements on liquid crystal polymer for MIMO," in *Proc. IEEE Int. Symp. Phased Array Syst. Technol. (PAST)*, 2019, pp. 1–5.

[2] M. Schwartz, W. R. Bennett, and S. Stein, *Communication Systems and Techniques*. New York, NY, USA: McGraw-Hill, 1965.

[3] W. Jakes, *Microwave Mobile Communications*. New York, NY, USA: Wiley, 1974.
[4] R. G. Vaughan and J. B. Andersen, "Antenna diversity in mobile communications," *IEEE Trans. Veh. Technol.*, vol. 36, no. 4, pp. 149–172, Nov. 1987.
[5] W. C.-Y. Lee, "Antenna spacing requirement for a mobile radio basestation diversity," *Bell Syst. Tech. J.*, vol. 50, no. 6, pp. 1859–1876, Jul./Aug. 1971.
[6] R. G. Vaughan, "Polarization diversity in mobile communications," *IEEE Trans. Veh. Technol.*, vol. 39, no. 3, pp. 177–186, Aug. 1990.
[7] R. G. Vaughan and N. L. Scott, "Closely spaced monopoles for mobile communications," *Radio Sci.*, vol. 28, no. 6, pp. 1259–1266, 1993.
[8] M. A. Jensen and J. W. Wallace, "A review of antennas and propagation for MIMO wireless communications," *IEEE Trans. Antennas Propag.*, vol. 52, no. 11, pp. 2810–2824, Nov. 2004.
[9] Y. Sankarasubramaniam, I. F. Akyildiz, W. Su, and E. Cayirci, "Wireless sensor networks: A survey," *Comput. Netw.*, vol. 38, no. 4, pp. 393–422, Mar. 2002.
[10] Y.-P. E. Wang *et al.*, "A primer on 3GPP narrowband Internet of Things," *IEEE Commun. Mag.*, vol. 55, no. 3, pp. 117–123, Mar. 2017.
[11] C. G. Hynes and R. G. Vaughan, "A benchmark for antenna correlation measurements," *IEEE Trans. Antennas Propag.*, vol. 68, no. 9, pp. 6624–6635, Sep. 2020.
[12] M. Razmhosseini and R. G. Vaughan, "Diversity design in wireless communications," in *Proc. Int. Conf. Workshop Comput. Commun. (IEMCON)*, Oct. 2015, pp. 1–6.
[13] R. G. Vaughan and J. B. Andersen, *Channels, Propagations and Antennas for Mobile Communications*, 1st ed. London, U.K.: Inst. Electr. Eng., 2003.
[14] A. Bhattacharya and R. G. Vaughan, "The antenna correlation coefficient in wireless sensor networks," in *Proc. 32nd URSI Gen. Assembly Sci. Symp. (URSI GASS)*, 2017, pp. 19–26.
[15] I. Salonen and P. Vainikainen, "Estimation of signal correlation in antenna arrays," in *Proc. 12th Int. Symp. Antennas*, 2002, pp. 383–386.
[16] S. Blanch, J. Romeu, and I. Corbella, "Exact representation of antenna system diversity performance from input parameter description," *Electron. Lett.*, vol. 39, no. 9, pp. 705–707, May 2003.
[17] R. G. Vaughan, "Antenna evaluation for communications with diversity/MIMO," in *Printed Antennas for Wireless Communications*, 1st ed., R. B. Waterhouse, Ed. West Sussex, U.K.: Wiley, 2007.
[18] J. X. Yun and R. G. Vaughan, "Multiple element antenna efficiency and its impact on diversity and capacity," *IEEE Trans. Antennas Propag.*, vol. 60, no. 2, pp. 529–539, Feb. 2012.
[19] J. Thaysen and K. Jakobsen, "Envelope correlation in (N, N) MIMO antenna array from scattering parameters," *Microw. Opt. Technol. Lett.*, vol. 48, no. 5, pp. 832–834, Mar. 2006.
[20] A. Stjernman, "Relationship between radiation pattern correlation and scattering matrix of lossless and lossy antennas," *Electron. Lett.*, vol. 41, no. 12, pp. 678–680, Jun. 2005.
[21] M. Razmhosseini and R. G. Vaughan, "Accuracy of modeling for evaluation of an integrated diversity wireless system on a small PCB," in *Proc. IEEE Int. Symp. Antennas Propag. USNC/URSI Natl. Radio Sci. Meeting*, Jul. 2015, pp. 1230–1231.
[22] T. Taga, "Analysis for mean effective gain of mobile antennas in land mobile radio environments," *IEEE Trans. Veh. Technol.*, vol. 39, no. 2, pp. 117–131, May 1990.
[23] O. Norklit and R. G. Vaughan, "Method to determine effective number of diversity branches," in *Proc. IEEE GLOBECOM*, vol. 1, Nov. 1998, pp. 138–141.
[24] K. Ogawa and J. Ichi Takada, "An analysis of the effective performance of a handset diversity antenna influenced by head, hand, and shoulder effects—A proposal for a diversity antenna gain based on a signal bit-error rate and analytical results for the PDC system," *Inst. Electron. Inf. Commun. Eng.*, vol. 84, no. 6, pp. 10–23, Jun. 2001.
[25] R. G. Gallager, *Information Theory and Reliable Communication*. New York, NY, USA: Wiley, 1968.
[26] J. Winters, "On the capacity of radio communication systems with diversity in a rayleigh fading environment," *IEEE J. Sel. Areas Commun.*, vol. 5, no. 5, pp. 871–878, Jun. 1987.
[27] D.-S. Shiu, G. J. Foschini, M. J. Gans, and J. M. Kahn, "Fading correlation and its effect on the capacity of multielement antenna systems," *IEEE Trans. Commun.*, vol. 48, no. 3, pp. 502–513, Mar. 2000.
[28] S. A. Banani and R. G. Vaughan, "Blind channel estimation and discrete speed tracking in wireless systems using independent component analysis with particle filtering," *IET Commun.*, vol. 6, no. 2, pp. 224–234, Jan. 2012.
[29] *MIMObit*, Accessed: Apr. 21, 2019. [Online]. Available: http://www.nebens.com/home/products
[30] *AT&T Radiated Performance Requirements*. Accessed: Sep. 28, 2019. [Online]. Available: https://iotdevices.att.com/Uploaded_Docs/radiated_performance_requirements_20180530134303267.pdf
[31] J. Rahola, "Power waves and conjugate matching," *IEEE Trans. Circuits Syst. II, Exp. Briefs*, vol. 55, no. 1, pp. 92–96, Jan. 2008.
[32] M. Razmhosseini, A. Bhattacharya, and R. G. Vaughan, "Benchmark diversity results for generic spaced patch antennas," in *Proc. 18th Int. Symp. Antenna Technol. Appl. Electromagn. (ANTEM)*, Aug. 2018, pp. 1–2.
[33] M. Manteghi and Y. Rahmat-Samii, "Broadband characterization of the total active reflection coefficient of multiport antennas," in *IEEE Antennas Propag. Soc. Int. Symp.*, vol. 3, Jun. 2003, pp. 20–23.
[34] S. H. Chae, S. K. Oh, and S.-O. Park, "Analysis of mutual coupling, correlations, and TARC in Wibro MIMO array antenna," *IEEE Antennas Wireless Propag. Lett.*, vol. 6, pp. 122–125, Apr. 2007.
[35] S. H. Chae, W. I. Kawk, S.-O. Park, and K. Lee, "Analysis of mutual coupling in MIMO antenna array by TARC calculation," in *Proc. Asia-Pac. Microw. Conf.e*, Dec. 2006, pp. 2090–2093.
[36] (2017). *CST Microwave Studio*. [Online]. Available: https://www.cst.com/
[37] M. Razmhosseini, A. Bhattacharya, and R. G. Vaughan, "Chassis diversity antenna comparison," in *Proc. IEEE Int. Symp. Antennas Propag. USNC/URSI Natl. Radio Sci. Meeting*, Jul. 2018, pp. 1531–1532.
[38] L. Liu, Y. F. Weng, S. W. Cheung, T. I. Yuk, and L. J. Foged, "Modeling of cable for measurements of small monopole antennas," in *Proc. Loughborough Antennas Propag. Conf.*, 2011, pp. 1–4.
[39] J. Villanen, J. Ollikainen, O. Kivekas, and P. Vainikainen, "Compact antenna structures for mobile handsets," in *Proc. IEEE 58th Veh. Technol. Conf. (VTC-Fall)*, vol. 1, Oct. 2003, pp. 40–44.
[40] M. Dehghani Estarki, M. Razmhosseini, A. Bhattacharya, Y. Chen, C. Tumpach, L. Vishloff, and R. G. Vaughan, "Improvement of outage by retrofit of antenna diversity for MIMO on a PCB M2M system," in *Proc. IEEE Int. Symp. Antennas Propag. USNC/URSI Natl. Radio Sci. Meeting*, Jul. 2015, pp. 1224–1225.
[41] J. Ren and R. G. Vaughan, "Spaced antenna design in directional scenarios using the von Mises distribution," in *Proc. IEEE 70th Veh. Technol. Conf. Fall*, Sep. 2009, pp. 1–5.
[42] N. Jamaly, A. Derneryd, and Y. Rahmat-Samii, "A revisit to spatial correlation in terms of input network parameters," *IEEE Antennas Wireless Propag. Lett.*, vol. 11, pp. 1342–1345, Oct. 2012.
[43] J. X. Yun and R. G. Vaughan, "Space efficiency of multiple element antennas," *IEEE Trans. Antennas Propag.*, vol. 60, no. 6, pp. 3066–3071, Jun. 2012.

MARYAM RAZMHOSSEINI (Student Member, IEEE) received the B.Eng. degree in computer systems engineering and the M.Sc. degree in communication engineering and signal processing from Cardiff University, U.K., in 2008 and 2010, respectively. She is currently pursuing the Ph.D. degree with Simon Fraser University, Burnaby, BC, Canada. During her graduate studies, she worked on measurement of microwave resonators, design of spatial notch filters for beamforming, antennas for diversity/MIMO, and slot elements and arrays. She has also been involved in many antenna measurements campaigns for companies like SpaceX, Urthecast, and Norsat. Her current research interests include theory and design of antennas for diversity and MIMO communications, antenna measurements, and slot antennas.

ABHIJIT BHATTACHARYA (Member, IEEE) received the bachelor's and master's degrees in electronics and communications engineering in 2001 and 2005 respectively, and the Ph.D. degree from Simon Fraser University, Burnaby, BC, Canada, in 2020. Before his doctoral endeavors, he spent several years in the wireless communications industry working for Sierra Wireless Inc., and few others, designing antennas and radio frequency components for applications ranging from cellular base stations and wireless backhauls to portable mobile devices. He is currently as a Staff Engineer with Swiftlink Technologies., Inc., Vancouver, BC, he is involved in designing antennas and arrays for 5G mm-wave applications. His current research interests include antenna theory and design, mm-wave circuits and antennas, electronically scanned arrays, and applications of deep-learning in 5G wireless.

RODNEY G. VAUGHAN (Life Fellow, IEEE) is the Sierra Wireless Professor in Communications with Engineering Science, SFU. His university training was in New Zealand and Denmark. Most of his career has involved industrial development where the value of research ultimately drew him to academia. His research revolves round information channels and the interplay between communications techniques, signal processing, and the physical aspects–the sensors, and the propagation and scattering of fields and waves. Current projects include theory, design and evaluation methods for adaptive antenna systems and adaptive acoustic systems. He is a 2004 Fellow of the BC Advanced System Institute, an URSI Correspondent, and continues as the New Zealand URSI Commission B representative. In 2006, he served on the international panel for reviewing the funding and knowledge base for ICT in the U.K., and in 2011 for the Canadian Communications Research Centre, and also for the ICT Centre of the CSIRO. He has been an Associate Editor for the IEEE TRANSACTIONS ON ANTENNAS AND PROPAGATION and has a Guest-Edited Special Issues. He was a multiterm IEEE Distinguished Lecturer for the Vehicular Technology Society, and has had the Chair roles for IEEE conferences.